THE JOURNAL OF PHYSICAL CHEMISTRY C

Article

pubs.acs.org/JPCC

Thermal Evolution of Cation Distribution/Crystallite Size and Their Correlation with the Magnetic State of Yb-Substituted Zinc Ferrite Nanoparticles

M. Vucinic-Vasic,[†] E. S. Bozin,[‡] L. Bessais,[§] G. Stojanovic,[†] U. Kozmidis-Luburic,[†] M. Abeykoon,[‡] B. Jancar,[∥] A. Meden,[⊥] A. Kremenovic,[#,▽] and B. Antic*[,#]

[†]Faculty of Technical Sciences, University of Novi Sad, Trg D. Obradovica 6, 21000 Novi Sad, Serbia

[‡]Condensed Matter Physics and Materials Science Department, Brookhaven National Laboratory, Upton, New York 11973, United States

[§]ICPME, UMR 7075 CNRS and Université Pierre and Marie Curie, 94230 Thiais, France

[∥]Jožef Štefan Institute, Jamova 39, 1000 Ljubljana, Slovenia

[⊥]Faculty of Chemistry and Chemical Technology, University of Ljubljana, 1000 Ljubljana, Slovenia

[#]Institute of Nuclear Sciences "Vinča", University of Belgrade, P.O. Box 522, 11001 Belgrade, Serbia

[▽]Faculty of Mining and Geology, Laboratory for Crystallography, University of Belgrade, P.O. Box 162, 11001 Belgrade, Serbia

ABSTRACT: Evolution of the structural and magnetic properties of $ZnFe_{1.95}Yb_{0.05}O_4$ nanoparticles, prepared via a high-energy ball milling route and exposed to further thermal annealing/heating, was assessed in detail and correlation of these properties explored. While as-prepared spinel nanoparticles possess a high degree of inversion, heating of the sample to ∼500 °C is found to rapidly alter the cation distribution from mixed to normal, in agreement with the known cation preferences. Under the same conditions the crystallite size only slowly grows. By further thermal treatment at higher temperatures, the crystallite size is changed more appreciably. An interrelationship among the lattice parameter, octahedral site occupancy, and crystallite size has been established. The observations are (a) both the site occupancy of Fe^{3+} at octahedral 16d spinel sites ($N_{16d}(Fe^{3+})$) and the cubic lattice parameter rapidly increase with an initial increase of the crystallite size, (b) the lattice parameter increases with increasing occupancy, $N_{16d}(Fe^{3+})$, and (c) there appears to be a critical nanoparticle diameter (approximately 15 nm) above which both the site occupancy and lattice parameter values are saturated. The magnetic behavior of the annealed samples appears to be correlated to the evolution of both the cation distribution and crystallite size, as follows. As-prepared samples and those annealed at lower temperatures show superparamagnetic behavior at room temperature, presumably as a consequence of the Fe^{3+} distribution and strong Fe^{3+}(8a)−O−Fe^{3+}(16d) superexchange interactions. Samples with a nanoparticle diameter greater than 12 nm and with almost normal distributions exhibit the paramagnetic state. The coercive field is found to decrease with an increase of the crystallite size. Partial Yb^{3+}/Fe^{3+} substitution is found to increase the inversion parameter and saturation magnetization. Detailed knowledge of the thermal evolution of structural/microstructural parameters allows control over the cation distribution and crystallite size and hence the magnetic properties of nanoferrites.

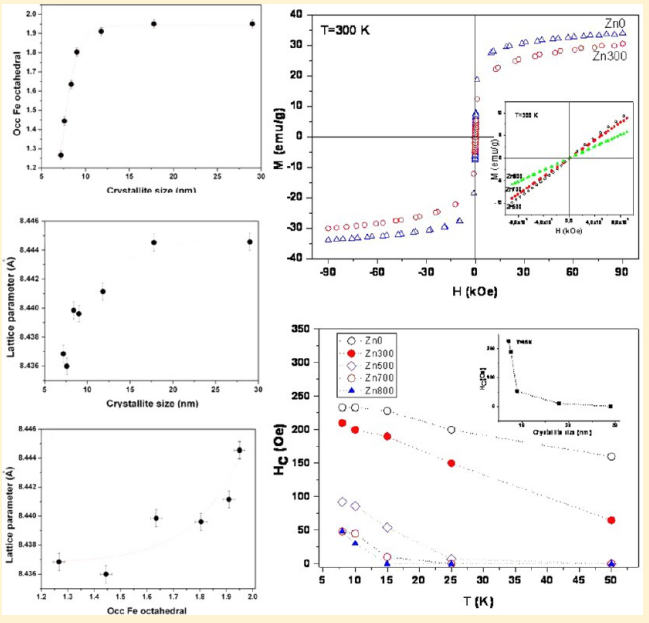

1. INTRODUCTION

For many years ferrites have been one of the most studied materials, particularly in the form of nanopowders and thin films. They crystallize in a simple spinel structure and often serve as model systems. Their broad industrial applications require development of controlled methods for their synthesis, which would supply the targeted characteristics of the material. Another possibility to optimize the physical properties of a ferrite is a partial substitution of cations by 3d and 4f elements. The rare earth (4f) ions are larger than the hosts; hence, they often create

Received: April 8, 2013
Revised: May 12, 2013
Published: May 15, 2013

ACS Publications © 2013 American Chemical Society

structural distortions and have significant influence on the crystallite strain. Binary ferrites (MFe_2O_4; M = Zn, Mn, Fe, Ni, Cr) are often doped/substituted to improve their magnetic properties. It is noteworthy that a series of $Fe_{2.85}RE_{0.15}O_4$ (RE = Gd, Dy, Ho, Tm, and Yb) samples have recently been prepared by high-energy ball milling (HEBM) protocols, and a correlation between the magnetic and structure properties has been reported.[1] One of the goals of this study is to investigate the effect of partial substitution of Fe ions with Yb in the zinc ferrite nanoparticle system on the magnetic properties of the parent compound.

Ferrites crystallize in a spinel-type cubic structure, which is traditionally divided into two different ideal structure types, normal and inverse. In normal spinels, M ions of ferrites MFe_2O_4 are solely located on tetrahedral (8a) sites and Fe ions solely on octahedral (16d) sites within the $Fd\bar{3}m$ space group. Inverse spinels have half of the Fe ions residing on tetrahedral sites, while the rest of the Fe ions and all the M ions occupy the octahedral sites. At the nanoscale, the cation distribution is often found to be mixed (between these two ideal structure types), and this is then quantified by the inversion parameter, which corresponds to the fraction of M ions residing on the octahedral sites. Bulk $ZnFe_2O_4$ is known to have an almost normal spinel structure with Zn^{2+} ions located on tetrahedral sites and Fe^{3+} ions located on the octahedral sites. On the other hand, the nanosized counterpart has a mixed cation distribution $(Zn_{1-\alpha}Fe_\alpha)_{8a}[Zn_\alpha Fe_{2-\alpha}]_{16d}$, where the inversion parameter α is found to vary, depending on the sample preparation method and the thermal treatment.[2]

The aims of this work were (i) the synthesis of Yb-substituted zinc ferrite by the HEBM method, (ii) an investigation of the thermal evolution of structural and microstructural parameters by both in situ and ex situ X-ray diffraction techniques, (iii) the determination of the magnetic properties of as-prepared and annealed samples, and (iv) an investigation of the relationship between the structure/microstructure and the magnetic properties.

2. EXPERIMENTAL SECTION

2.1. Mechanochemical Synthesis. The starting compounds for mechanochemical synthesis of the title compound were ZnO, Fe_2O_3, and Yb_2O_3. They were mixed in appropriate molar ratios according to the stoichiometry $ZnFe_{1.95}Yb_{0.05}O_4$. The mixture was milled in air using a planetary ball Fritch "pulverizette 4" mill equipped with tungsten carbide bowls and balls. The milling parameters were a ball-to-powder mass ratio of 20:1, a rotation speed of the main disk of 400 rpm, and a rotation speed of the planets of 1300 rpm. Balls 10 mm in diameter and a 250 mL bowl were used. The time of milling was approximately 10 h.

As-prepared $ZnFe_{1.95}Yb_{0.05}O_4$ (Zn0) from the same batch was then annealed at different temperatures (300, 400, 500, 600, 700, and 800 °C) for 6 h each. The annealed samples are labeled as Zn300, Zn400, Zn500, Zn600, Zn700, and Zn800, where the numbers denote the corresponding annealing temperature.

2.2. Experimental Methods: X-ray Diffraction (XRD), Transmission Electron Microscopy (TEM), and Electrical and Magnetization Measurements. X-ray powder diffraction (XRPD) data were collected on a PANalytical X'pert PRO diffractometer equipped with an Anton Paar HTK-1200N using Cu $K\alpha_1$ radiation. Data were collected in the 2θ range from 16.995° to 89.976° in steps of 0.053° for in the situ regime and from 15.019° to 119.941° in steps of 0.067° for the ex situ regime. In situ measurements were made at room temperature and in the temperature interval of 100−600 °C in steps of 100 °C. Separately, after annealing at temperatures of 300, 400, 500, 600, 700, and 800 °C, the diffraction patterns on such obtained samples were collected at room temperature (ex situ regime).

The synchrotron X-ray experiment was conducted on ex situ samples at 300 K on the 11-IDC beamline of the Advanced Photon Source (APS) at Argonne National Laboratory (ANL). The setup utilized an X-ray beam 0.5 mm × 0.5 mm in size with a wavelength of 0.108 Å (E = 114.82 keV) and a Perkin-Elmer amorphous silicon image plate detector mounted perpendicular to the primary beam path. Finely pulverized samples packed in a cylindrical polyimide capillary 1 mm in diameter were placed 357.84 mm away from the detector. Multiple scans were performed on each sample to a total exposure time of 250 s to improve the counting statistics. The 2D diffraction data were integrated and converted to intensity versus 2θ data using the software FIT2D.[3] The intensity data were corrected and normalized[4] and converted to an atomic pair distribution function (PDF), $G(r)$, using the program PDFgetX2.[5] Data up to Q_{max} = 26 Å^{-1} were used in the Fourier transform, an optimal value found for this set of measurements balancing the trade-off between the signal-to-noise ratio and the counting statistics, to produce good-quality PDFs.[4]

Transmission electron micrographs were collected with a Jeol JEM 2100 transmission electron microscope operating at 200 kV. The samples were prepared by dispersing the powders in acetone and dropping the suspension on a lacey carbon film supported on a 300-mesh copper grid.

Magnetic measurements were performed on a PPMS magnetometer. Magnetization vs field, $M(H)$, data were measured in the 10−300 K temperature range under the zero-field-cooled (ZFC) regime up to a field of 9 T.

3. RESULTS AND DISCUSSION

3.1. Crystal Structure Determination of $ZnFe_{1.95}Yb_{0.05}O_4$ by Rietveld Refinement and PDF Modeling. The prepared sample was checked using the collected XRD data. All the reflections in the diffraction pattern were indexed in the expected $Fd\bar{3}m$ space group and the spinel structure type. However, some low-intensity reflections were noticed originating from hematite and tungsten carbide. Contamination of tungsten carbide derived from the bowls and balls that were used in the synthesis process.

X-ray diffraction data collected at room temperature for as-prepared $ZnFe_{1.95}Yb_{0.05}O_4$ and annealed samples were used to refine the structure parameters to study their thermal evolution (ex situ studies). The evolution of the structure parameters with heating of the as-prepared Zn0 sample was also investigated using the in situ diffraction technique in the temperature range of 25−600 °C.

Due to the presence of hematite and tungsten carbide besides the main spinel phase, we have used a three-phase Rietveld refinement in the Fullprof computer program[6] to refine the crystal structure parameters. The refinement ascertained the weight fraction for both hematite and tungsten carbide (WC) phases together to be less than 1.5 wt % (ex situ). Figure 1 shows the graphical result of the Rietveld refinement procedure for Zn0 with a comparison between observed and calculated intensities. Tungsten carbide reflections were not visible in the diffraction pattern of samples annealed at 500 °C and higher temperatures (ex situ studies) or at temperatures above 500 °C (in situ studies). It is well-known that tungsten carbide powder burns in air. Oxidation of WC powder starts at 500 °C, and WC can be burned completely at 529 °C.[7] Structural parameters of the main ferrite phase that were refined were the lattice parameter, isotropic temperature factors, and occupation numbers.

dx.doi.org/10.1021/jp403459t | J. Phys. Chem. C 2013, 117, 12358−12365

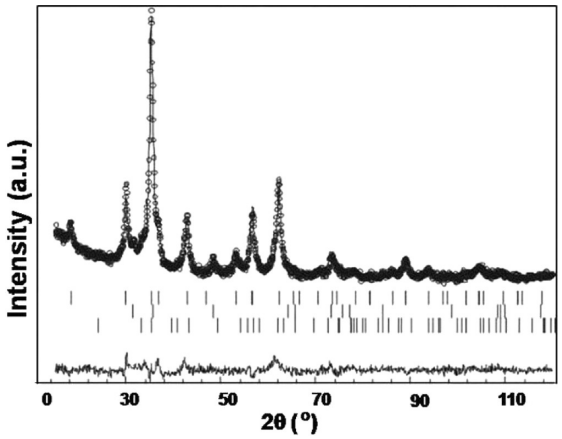

Figure 1. Representative final Rietveld refinement for the Zn0 sample, showing the comparison between observed (○) and calculated (solid line) step intensities, as well as their difference. The vertical bars indicate the positions of the crystallographic reflections for the individual phases used. From top to bottom, the first row of tick marks corresponds to the ferrite phase, the second to tungstene carbide, and the third to hematite.

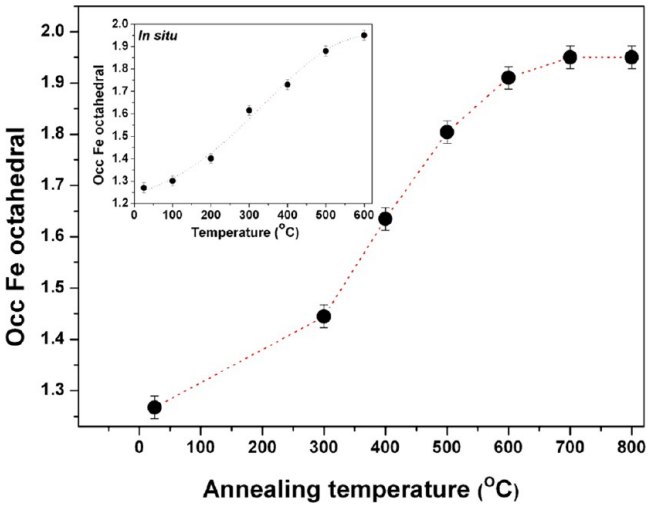

Figure 2. Occupation parameter of Fe^{3+} ions at octahedral sites versus the annealing temperature. The main panel corresponds to room temperature values obtained for the ex situ regime, while the inset shows this evolution in the in situ regime. Dashed lines are guides for the eyes.

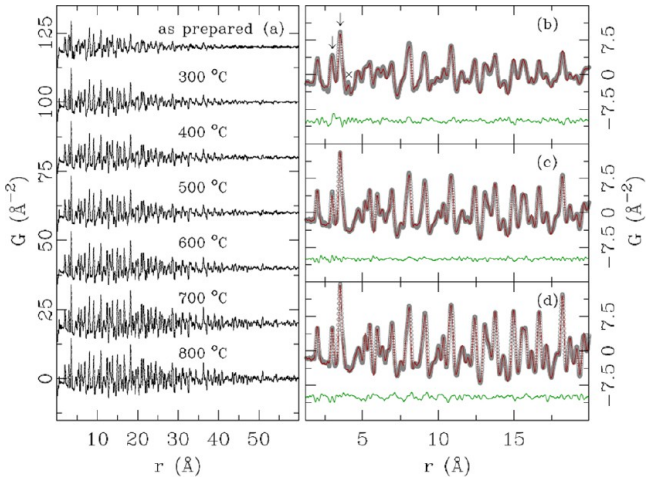

Figure 3. (a) Comparison of experimental PDFs at 300 K obtained from the ex situ experiment on the as-prepared and annealed samples. The annealing temperatures are noted next to the PDF profiles to which they correspond. (b) Fit of the two-phase model (cubic $Fd\bar{3}m$ phase and the WC impurity phase discussed in the text) to the data of the as-prepared sample. Open symbols are the data, the red solid curve is the model, and the green line is the difference that is offset for clarity. Features marked by arrows and a times sign are discussed in the text. (c) and (d) show single-phase $Fd\bar{3}m$ model fits to the data of the samples annealed at 400 and 800 °C, respectively.

The cation distribution was determined by refinement of site occupancies in the Rietveld approach. The starting model for Rietveld refinement was a random cation distribution of Zn^{2+} and Fe^{3+} ions at octahedral and tetrahedral sites. All Yb^{3+} ions were placed in octahedral sites and fixed there, due to the known Yb^{3+} preference for the octahedral site as well as due to the relatively small atomic fraction of Yb in $ZnFe_{1.95}Yb_{0.05}O_4$. Site occupancies of Zn and Fe were constrained to keep the stoichiometric ratio. Refined cation site occupancy values for the as-prepared sample denoted a mixed distribution, $(Zn_{0.32}Fe_{0.68})_{8a}[Zn_{0.68}Fe_{1.27}Yb_{0.05}]_{16d}$. The found inversion parameter of 0.68 denotes a very high level of inversion. It is important to note that in $ZnFe_2O_4$ prepared following the same protocols the inversion parameter was found to be 0.43.[8] In mechanochemical synthesis of ferrites, cations can be distributed against their known site preferences (in a large percentage), influencing the physical properties significantly; see, e.g., ref 9. The influence of partial substitution of Fe^{3+} by Yb^{3+} on the cation distribution probably is one of the main reasons for high inversion. To overcome the shortcomings of the Rietveld method for determination of the cation distribution, computed cation−anion bond lengths (based on the values of the Shannon ionic radii) were then compared with those obtained from the refined structure geometry parameters. Final distributions were established when satisfactory agreement between the bond lengths calculated using the two approaches was achieved.

The thermal evolution of the cation distribution is shown in Figure 2 using the values of the occupation number for Fe in octahedral 16d positions. Both ex situ and in situ values show the same tendency to change. Specifically, the distribution appears to exhibit significant changes from mixed toward normal with annealing/heating at lower temperatures (up to 500 °C). With further increasing the annealing temperature to 800 °C, the distribution is slowly changed to normal.

In addition to the crystallographic approach, another approach to analyze the effects of thermal annealing on the structural parameters was used. The experimental PDFs of as-prepared and annealed samples are shown in Figure 3a. As can be seen, the intensity is attenuated at high values of r due to the finite particle size. As the particle size grows, the PDF peaks become more intense at high r and the features propagate further. The PDF structural analysis was carried out using the program PDFgui.[5]

The data for all samples are explained reasonably well within the cubic spinel model having $Fd\bar{3}m$ symmetry. The model utilizing eight independent parameters (lattice parameter, oxygen fractional coordinate, iron occupancy in the 16d position, three isotropic atomic displacement parameters, nanoparticle diameter assuming a spherical particle shape, and an overall scale factor) was refined over the 1.2−50 Å range. The occupancy of the 16d site was set to values obtained from the combined approach described above and kept fixed. Representative final fits over a selected range are shown in Figure 3 b−d for the as-prepared sample and samples annealed at 400 and 800 °C, respectively. The fit to the data of the as-prepared sample was substantially worse than the others. A two-phase fit was necessary to account

dx.doi.org/10.1021/jp403459t | J. Phys. Chem. C 2013, 117, 12358−12365

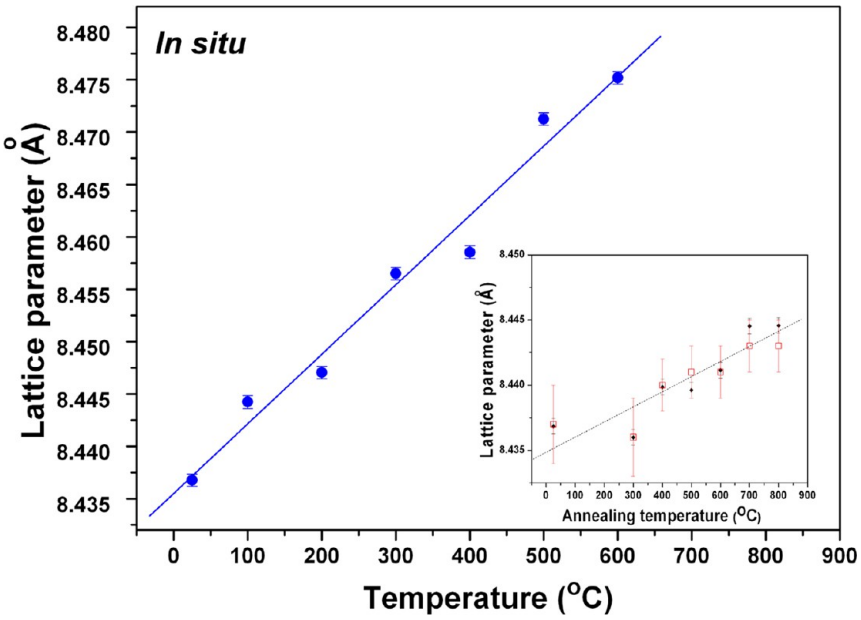

Figure 4. Linear fit to the lattice parameter for as-prepared $ZnFe_{1.95}Yb_{0.05}O_4$ as a function of temperature (in situ) and annealing temperature in the inset (ex situ, Rietveld results are presented by squares, PDF results by tilted squares).

for the presence of the tungsten carbide residue. A feature from this phase can be seen in Figure 3 b marked by a times sign. Closer examination of the difference curve reveals the existence of discrepancies in the low-r region of the PDF for the as-prepared nanocrystalline sample that the $Fd\bar{3}m$ model does not capture correctly. Furthermore, comparison of atomic displacement parameters (ADPs) obtained from broad-range refinement of the as-prepared sample data relative to those obtained for the annealed samples indicates enlarged values of ADPs for all three atomic species in the as-prepared specimen. This is also observed as markedly broader PDF peaks in Figure 3 b compared to the corresponding peaks seen in the data shown in Figure 3 c,d. While the cubic model in principle explains the data over a broad range, it misses the positions of the PDF peaks centered at around ~3.0 and ~3.5 Å, marked by arrows in Figure 3 b. The two peaks correspond to the near-neighbor Fe−Fe (16d−16d) and Zn−Zn (8a−8a) distances in the $Fd\bar{3}m$ structure, respectively. This is a known local structural effect caused by an appreciable degree of inversion, as seen in zinc ferrites by the extended X-ray absorption fine structure (EXAFS),[10] X-ray absorption near-edge structure (XANES),[11] and PDF,[12] and was discussed in detail elsewhere.[12] This effect is not observed in the data of the annealed samples. Also, the WC impurity is not observed in the data of these samples.

In Figure 4, the change of the lattice parameter with thermal annealing/heating is shown. The lattice parameter of the as-prepared sample shows an approximately linear dependence on the temperature (main panel). The parameters of linear tendency $a = a_0 + kt$ were $a_0 = 8.435(2)$ Å and $k = 6.6(5) \times 10^{-5}$ Å/°C. Lattice parameter changes for the in situ regime are related to (i) simple thermal expansion, (ii) the changes in the cation distribution, (iii) the crystallite size effects (grain−surface relaxation effect), and (iv) the valence of the polyvalent ions. The inset of Figure 4 shows the room temperature lattice parameters determined by the Rietveld and PDF approaches of the annealed samples (ex situ regime). The unit cell changes in this case are related to effects ii−iv. The change of lattice parameter due to changes in the cation distribution is based on migration of cations between tetrahedral and octahedral sites. The lattice parameter of the spinel lattice depends on the complex interplay between the size of the ions and their distribution. Ionic radii for tetrahedral (IV) and octahedral (VI) coordination are Fe^{3+}(IV) = 0.49 Å, Fe^{3+}(VI) = 0.645 Å, Zn^{2+}(IV) = 0.60 Å, Zn^{2+}(VI) = 0.745 Å, Yb^{3+}(VI) = 0.858 Å, and O^{2-}(IV) = 1.38 Å.[13] The unit cell parameters of most nanocrystalline materials can also be significantly different from the coarse-grain or single-crystal counterparts due to the grain−surface relaxation effect.[14] The possible reduction of iron from the +3 to the +2 state could also influence the lattice parameter due to the difference in their ionic radius. The difference in the values of the lattice parameter of the annealed sample at a certain temperature and the as-prepared sample heated at the same temperature is a result of thermal expansion and partial differences in the distribution of cations in the 8a and 16d sites. The relative difference between the occupancies of iron at octahedral sites for the two regimes (in situ and ex situ) is equal to or smaller than 5%, except at a temperature of 300 °C, for which the difference is about 10%. Using the obtained values of the lattice parameter for the in situ regime, we can calculate the linear thermal expansion coefficient. The obtained value is $\alpha = 6.4(6) \times 10^{-6}$ °C^{-1}. Literature data for the linear thermal expansion coefficient of bulk and nanocrystalline $ZnFe_2O_4$ are 6.959×10^{-6} °C^{-1} [15] and 7.1×10^{-6} °C^{-1},[9] respectively. The coefficient of volume thermal expansion, $\beta = 3\alpha = 1.9(1) \times 10^{-5}$ °C^{-1}, is in reasonably good agreement with the value (2.056×10^{-5} °C^{-1}) calculated using Ottonelo's empirical formula with the oxygen fractional coordinate set to $u = 0.385$.[16]

3.2. Microstructure Analysis and Correlations between Structure−Microstructure Parameters. Crystallite size values were obtained by standard line profile analysis of the XRPD data using the Fullprof program. X-ray line broadening was analyzed by refining regular TCH-pV function parameters (isotropic effects).[17] The annealing temperature dependent crystallite size is shown in Figure 5, with the corresponding temperature dependence for the in situ regime shown in the inset. While the crystallite sizes of the samples annealed at

dx.doi.org/10.1021/jp403459t | J. Phys. Chem. C 2013, 117, 12358−12365

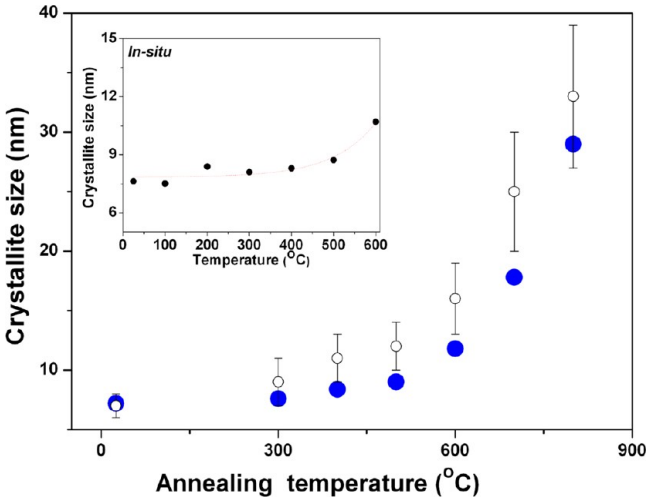

Figure 5. Dependence of the crystallite size for $ZnFe_{1.95}Yb_{0.05}O_4$ on the annealing temperature (●, Rietveld results; ○, PDF results). Inset: evolution of the crystallite size of the as-prepared sample with temperature (in situ studies). The line is a guide for the eyes.

temperatures up to 500 °C are found to be rather similar, slowly increasing between ∼7 and 9 nm, for the samples annealed at higher temperatures the crystallite size increases much more rapidly. Such a tendency in the evolution of the crystallite size with the annealing conditions assessed from room temperature data was obtained by both the Rietveld and PDF approaches. The in situ assessment by heating the as-prepared sample is in agreement with this, revealing that the crystallite size is almost constant (7.5−8.7 nm) up to 500 °C and then shows an increasing tendency at higher temperature.

To better understand the physical properties of the studied nanoparticles, it is of importance to compare side by side the details of the temperature evolution of various structural−microstructural parameters, including the crystallite size, cation distribution, and lattice parameters, and explore their correlations. At lower heating/annealing temperatures the crystallite size increases rather slowly. In contrast, in the same temperature regime, the migration of cations happens quite quickly. Variation of the lattice parameter with temperature appears to be linear. Thus, for samples annealed at lower temperatures, the dominant effect on the physical properties is likely due to the cation redistribution. On the other hand, at higher processing temperatures the cation distribution becomes close to normal and does not change appreciably anymore, so the samples annealed at temperatures at and above 600 °C can be used to examine the effects of the particle size on the observed physical properties. Figure 6 summarizes the relationship between the crystallite size and the corresponding cation distribution and lattice parameter, as derived from structural refinements of data in the ex situ regime. This analysis reveals that the crystallite size has a rather dramatic effect on both the cation distribution and lattice parameters for sizes below ∼10 nm, Figure 6 a,b. On the other hand, values of the occupancies and lattice parameters appear to be saturated to approximately their bulk-counterpart values for crystallites larger than ∼15 nm. It is tempting to speculate that ∼15 nm is a threshold diameter beyond which the size effect on the cation distribution and lattice parameters becomes less important. With increasing particle size, migration of the cations happens very quickly. Figure 6c shows a trend of increasing lattice parameters with increasing population of the

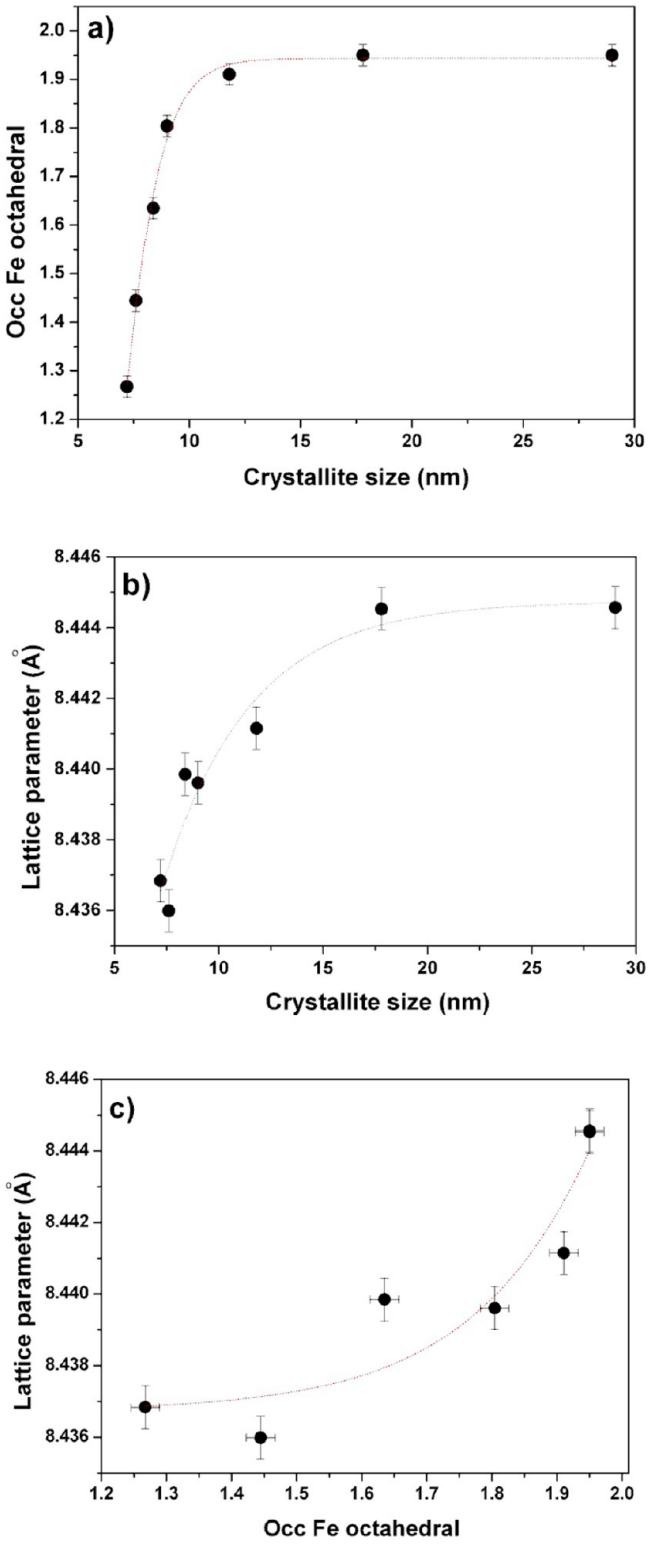

Figure 6. Relationship between (a) the occupation parameter of Fe^{3+} ions at octahedral sites and the crystallite size, (b) the lattice parameter and the crystallite size, and (c) the lattice parameter and the occupation parameter of Fe^{3+} ions at octahedral sites. Refined structural parameters of the annealed samples are used. The lines are guides for the eyes.

octahedral sites by iron ions, reflecting the difference in the respective zinc and iron ionic radii involved in cation rearrangement between the octahedral and tetrahedral sites in the spinel.

dx.doi.org/10.1021/jp403459t | J. Phys. Chem. C 2013, 117, 12358−12365

The morphology and particle size for the samples studied (ex situ, Zn0−Zn800) were assessed by TEM. These results are illustrated by selected TEM images of Zn0, Zn500, and Zn800 samples, shown in Figure 7. The particles appear to be nearly

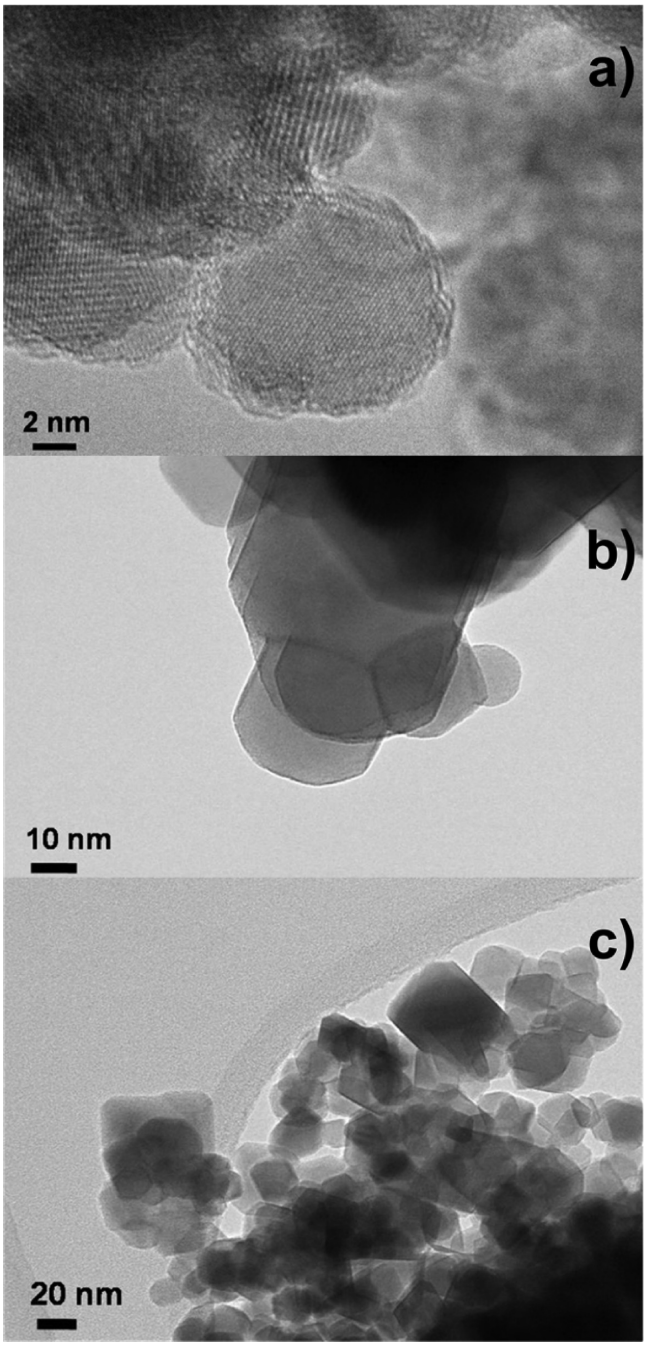

Figure 7. Representative TEM images of selected samples: (a) as-prepared, (b) annealed at 500 °C, and (c) annealed at 800 °C.

spherical in shape, with an average particle size of approximately 20 nm for samples Zn0−Zn300 and approximately 30 nm for samples Zn500−Zn800. Comparison of the Zn0−Zn800 results from TEM imaging, which reveals the overall particle shape and morphology (including conglomeration), and XRPD, which is sensitive to coherent structural cores of underlying nanocrystallites, suggests that as-prepared and annealed nanoparticles are composed of a few crystallites.

3.3. Hysteresis Loops in $ZnFe_{1.95}Yb_{0.05}O_4$. Magnetic hysteresis loops, $M(H)$, for the as-prepared sample (Zn0) as well as for a subset of the annealed samples (Zn300, Zn500, Zn700, Zn800) were recorded at 300 K, Figure 8. Observed

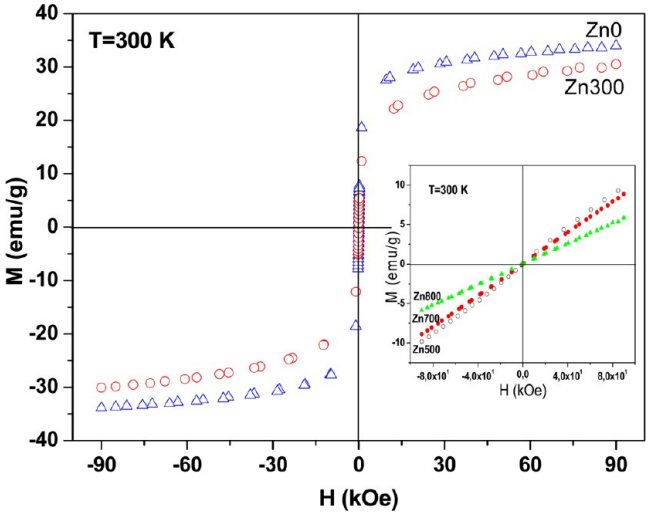

Figure 8. Magnetization versus applied magnetic field at 300 K for $ZnFe_{1.95}Yb_{0.05}O_4$ nanoparticles after annealing at different temperatures (see the text).

differences in $M(H)$ highlight the dependence of the magnetism of the studied system on the particle size and cation distribution. The S-shaped hysteresis loops with zero coercivity and remanence for the Zn0 and Zn300 samples point to their superparamagnetic behavior. For these samples magnetization is not saturated up to the maximum field of 9 T, which indicates enhanced magnetic anisotropy. The value of saturation magnetization, M_S, at room temperature was found to be 35 emu/g for Zn0, bigger than for mechanochemically synthesized zinc ferrite reported earlier, where M_S was found to be 30 emu/g.[18] Incorporation of a ytterbium ion in zinc ferrite influences the magnetocrystalline anisotropy and the value of the observed magnetization. Chinnasamy et al. have proposed that large magnetocrystalline anisotropy influences canting of the core spins and hence the magnetization value.[19] On the other hand, the $M(H)$ curves for the other three samples studied (Zn500, Zn700, and Zn800 corresponding to higher annealing temperatures) are typical for paramagnetic materials. We further elaborate on the $M(H)$ results to explore possible correlations between the magnetism and the structure−/microstructure.

It is well-known that bulk zinc ferrite shows antiferomagnetic behavior because of its normal spinel structure, with magnetic Fe^{3+} ions residing exclusively at 16d sites. However, in small-sized particles, cation redistribution occurs between 8a and 16d, sites leading to a mixed distribution, $(Zn_{1-x}Fe_x)_{8a}[Zn_xFe_{2-x}]_{16d}$. In that case magnetic behavior is determined by $(Fe^{3+})_{8a}$−O−$(Fe^{3+})_{16d}$-type interactions. In the case of as-prepared $ZnFe_{1.95}Yb_{0.05}O_4$, a rather large fraction of Fe^{3+} occupies 8a sites (as observed in Figure 2), causing ferrimagnetic order within single-domain nanoparticles. With annealing the sample at lower temperatures, this distribution is rapidly changed toward normal, while the particle size remains almost unchanged (Figure 5). Simultaneously, as observed, the magnetic behavior changes from superparamagnetic (Zn0, Zn300) to paramagnetic (Zn500, Zn700, Zn800). Correlation between the particle size and magnetism has been intensively investigated in a number of studies.[12] These results suggested that there is a critical

dx.doi.org/10.1021/jp403459t | J. Phys. Chem. C 2013, 117, 12358−12365

particle diameter at which they become single domain and display superparamagnetic behavior. As the particle size decreases, the surface effects become significant and impact the observed magnetic properties appreciably.[20] In sufficiently small particles, such as those studied in this work, a large fraction of spins are expected to be on the particle surface, and these spins have an influence on the net magnetic moment. The observed magnetic behavior is a consequence of both particle size and cation distribution effects. As shown in Figure 6, when the particle diameter reaches values on the order of ~15 nm, the cation distribution and lattice parameter become saturated. Interestingly, as the particle size is changed, the crossover in the observed magnetic properties where superparamagnetic behavior is seen appears to coincide with the characteristic diameter considered in structural−microstructural analysis. This indirectly points to the existence of correlation between the structural and magnetic properties.

To further understand the influence of the cation distribution and crystallite/particle size on the magnetism, we explored the temperature dependence of the coercivity, H_C, of these samples in the 10−300 K temperature range, as shown in Figure 9. For

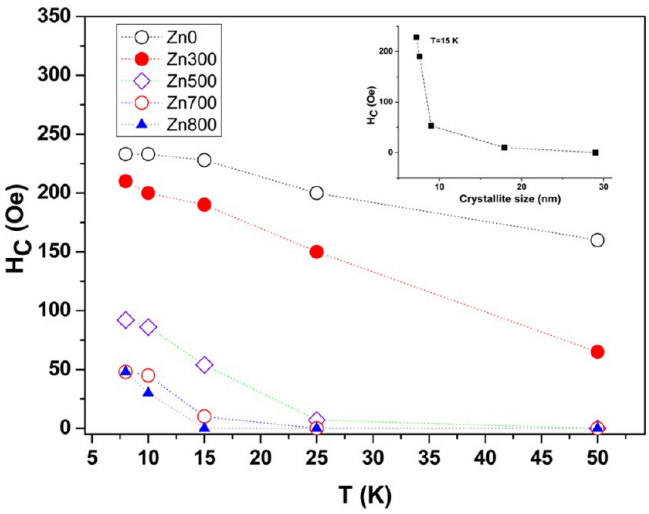

Figure 9. Coercive field (H_C) versus T for $ZnFe_{1.95}Yb_{0.05}O_4$ nanoparticles after annealing at various temperatures. The lines are guides for the eyes. Inset: dependence of H_C on the crystallite size at 15 K.

samples Zn0 and Zn300 coercivity has no zero value in this temperature range. Coercivity becomes zero at 25 K < T < 50 K for Zn500, at 15 K < T < 25 K for Zn700, and at 10 K < T < 15 K for Zn800, as can be seen in Figure 9. If the results are compared for two samples with approximately the same size, Zn300 and Zn500, the conclusion can be derived that the cation distribution dominates the particle size effects in its impact on the observed magnetic properties. To establish the particle size effect on the observed H_C value, a comparison can be made at fixed low temperature for all the samples studied. For this purpose we selected 15 K as a reference: at this temperature the H_C value sharply decreases with an increase of the crystallite size from Zn0 to Zn500 and becomes zero for Zn700. This is shown in the inset of Figure 9, where H_C is plotted versus the particle size at 15 K. For single-domain particles it is well-known that H_C initially increases with an increase of the crystallite size, but above specific characteristic dimensions, when the particles become multi-domain, H_C decreases.[21] However, the opposite behavior of H_C vs particle size has also been observed, as in, for example, nickel ferrite.[22] The enhancement of H_C in smaller nickel ferrite particles was attributed to the effect of spin canting that dominates the effect of the cation distribution.[22] The relationship between the crystallite size and coercivity in single-domain ferrite particles studied in this work is due to surface effects, possible structural disordering, and the cation distribution. Additionally, interparticle interactions also have a large effect on the magnetism. Their presence in the studied ensembles of ferrite nanoparticles is an inevitable reality.

4. CONCLUSION

$ZnFe_{1.95}Yb_{0.05}O_4$ nanoparticles were prepared using an inexpensive and simple mechanochemical procedure at room temperature. Successful substitution of Yb^{3+} for Fe^{3+} in a small percentage has been achieved. Although Yb^{3+} substitution into the spinel structure was done in a relatively small amount, the observed effects on the structural and magnetic properties are rather substantial, compared to those of the pure zinc ferrite system. Combined in situ and ex situ X-ray diffraction techniques, as well as two modeling approaches, Rietveld and PDF, were applied to determine the crystal structure and microstructure and to investigate their evolution with thermal treatment. For annealing/heating temperatures below 500 °C, the cation distribution rapidly changes, while the crystallite size increases rather slowly. The opposite trend is seen for the processing temperatures in the range between 500 and 800 °C. Knowledge of this structure−microstructure evolution allows tailoring the cation distribution and the crystallite size by application of appropriate thermal treatment of the as-prepared ferrite sample. Concerning the correlation of the structure−microstructure parameters and the magnetic properties, it was found that the cation distribution has a dominating influence on the magnetization and coercive field values over the particle size effects. Furthermore, this nanoparticle system appears to have an associated characteristic diameter of about 15 nm influencing the displayed magnetic properties. Particles with a larger diameter have saturated values of the cation distribution and lattice parameter. The results of this study also emphasize the importance of taking a systematic approach and combining multiple experimental techniques aimed at better understanding of complex nanocrystalline systems.

AUTHOR INFORMATION

Corresponding Author

*E-mail: bantic@vinca.rs.

Notes

The authors declare no competing financial interest.

ACKNOWLEDGMENTS

The Serbian Ministry of Education and Science has financially supported this work under Contract No. III45015. Work at Brookhaven National Laboratory was supported by the U.S. Department of Energy, Office of Science, Office of Basic Energy Sciences, under Contract No. DE-AC02-98CH10886. This work benefited from usage of the 11-IDC beamline of the APS at ANL. Use of the APS is supported by the U.S. Department of Energy, Office of Science, under Contract No. DE-AC02-06CH11357.

REFERENCES

(1) Cvejic, Z.; Antic, B.; Kremenovic, A.; Rakic, S.; Goya, G. F.; Rechenberg, H. R.; Jovalekic, C.; Spasojevic, V. Influence of Heavy Rare Earth Ions Substitution on Microstructure and Magnetism of Nanocrystalline Magnetite. *J. Alloys Compd.* **2009**, *472*, 571−575.

(2) Antic, B.; Kremenovic, A.; Nikolic, A. S.; Stoiljkovic, M. Cation Distribution and Size-Strain Microstructure Analysis in Ultrafine Zn−-Mn Ferrites Obtained from Acetylacetonato Complexes. *J. Phys. Chem. B* **2004**, *108*, 12646−12651.
(3) Hammersley, A. P.; Svenson, S. O.; Hanfland, M.; Hauserman, D. Two-Dimensional Detector Software: From Real Detector to Idealised Image or Two-Theta Scan. *High Pressure Res.* **1996**, *14*, 235−248.
(4) Egami, T.; Billinge, S. L. J. *Underneath the Bragg Peaks: Structural Analysis of Complex Materials*; Pergamon Press: Oxford, U.K., 2004.
(5) Qiu, X.; Thompson, J. W.; Billinge, S. J. L. PDFgetX2: A GUI Driven Program To Obtain the Pair Distribution Function from X-ray Powder Diffraction Data. *J. Appl. Crystallogr.* **2004**, *37*, 678−678.
(6) Rodriguez-Carvajal, J. FullProf computer program, 2009. http://www.ill.eu/sites/fullprof/ (accessed January 2010).
(7) Newkirk, A. E. The Oxidation of Tungsten Carbide. *J. Am. Chem. Soc.* **1955**, *77* (17), 4521−4522.
(8) Hofmann, M.; Campbell, S. J.; Ehrhardt, H.; Feyerherm, R. The Magnetic Behaviour of Nanostructured Zinc Ferrite. *J. Mater. Sci.* **2004**, *39*, 5057−5065.
(9) Philip, J.; Gnanaprakash, G.; Panneerselvam, G.; Antony, M. P.; Jayakumar, T.; Ray, B. Effect of Thermal Annealing under Vacuum on the Crystal Structure, Size, and Magnetic Properties of $ZnFe_2O_4$ Nanoparticles. *J. Appl. Phys.* **2007**, *102*, 054305.
(10) Ammar, S.; Jouini, N.; Fiévet, F.; Stephan, O.; Marhic, C.; Richard, M.; Villain, F.; Cartier dit Moulin, Ch.; Brice, S.; Sainctavit, Ph. Influence of the Synthesis Parameters on the Cationic Distribution of $ZnFe_2O_4$ Nanoparticles Obtained by Forced Hydrolysis in Polyol Medium. *J. Non-Cryst. Solids* **2004**, *345−346*, 658−662.
(11) Nakashima, S.; Koji Fujita, K.; Tanaka, K.; Hirao, K.; Yamamoto, T.; Tanaka, I. First-Principles XANES Simulations of Spinel Zinc Ferrite with a Disordered Cation Distribution. *Phys. Rev. B* **2007**, *75*, 174443.
(12) Antic, B.; Perovic, M.; Kremenovic, A.; Blanusa, J.; Spasojevic, V.; Vulic, P.; Bessais, L.; Bozin, E. S. An Integrated Study of Thermal Treatment Effects on the Microstructure and Magnetic Properties of Zn-Ferrite Nanoparticles. *J. Phys.: Condens. Matt.* **2013**, *25*, 086001.
(13) Shanon, R. D. Revised Effective Ionic Radii and Systematic Studies of Interatomic Distances in Halides and Chalcogenides. *Acta Crystallogr., A* **1976**, *32*, 751−767.
(14) Gleiter, H. Nanostructured Materials: Basic Concepts and Microstructure. *Acta Mater.* **2000**, *48*, 1−29.
(15) Šepelák, V.; Becker, K. D. Comparison of the Cation Inversion Parameter of the Nanoscale Milled Spinel Ferrites with That of the Quenched Bulk Materials. *Mater. Sci. Eng., A* **2004**, *375−377*, 861−864.
(16) Ottonello, G. Energetics of Multiple Oxides with Spinel Structure. *Phys. Chem. Mineral.* **1986**, *13*, 79−90.
(17) Honkimäki, V.; Surotti, P. In *Defect and Microstructure Analysis by Diffraction*; Snyder, R. L., Fiala, J., Bunge, H. J., Eds.; Oxford University Press: New York, 1999; pp 41−58.
(18) Lemine, O. M.; Bououdina, M.; Sajieddine, M.; Al-Saie, A. M.; Shafi, M.; Khatab, A.; Al-hilali, M.; Henini, H. Synthesis, Structural, Magnetic and Optical Properties of Nanocrystalline $ZnFe_2O_4$. *Physica B* **2001**, *406*, 1989−1994.
(19) Chinnasamy, C. N.; Narayanasamy, A.; Ponpandian, N.; Chattopadhyay, K.; Shinoda, K.; Jeyadevan, B.; Tohji, K.; Nakatsuka, K.; Furubayashi, T.; Nakatani, I. Mixed Spinel Structure in Nanocrystalline $NiFe_2O_4$. *Phys. Rev. B* **2001**, *63*, 184108−1−6.
(20) Yao, C.; Zeng, Q.; Goya, G. F.; Torres, T.; Liu, J.; Wu, H.; Ge, M.; Zeng, Y.; Wang, Y.; Jiang, J. Z. $ZnFe_2O_4$ Nanocrystals: Synthesis and Magnetic Properties. *J. Phys. Chem. C* **2007**, *111*, 12274−12278.
(21) Malik, R.; Annapoorni, S.; Lamba, S.; Sharma, P.; Inoue, A. Competing Magnetic Interactions in Nickel Ferrite Nanoparticle Clusters: Role of Magnetic Interactions. *J. Appl. Phys.* **2008**, *104*, 064317 and references therein.
(22) Sepelak, V.; Bergmann, I.; Feldhoff, A.; Heitjans, P.; Krumeich, F.; Menzel, D.; Litterst, F. J.; Campbell, S. J.; Becker, K. D. Nanocrystalline Nickel Ferrite, $NiFe_2O_4$: Mechanosynthesis, Nonequilibrium Cation Distribution, Canted Spin Arrangement, and Magnetic Behavior. *J. Phys. Chem. C* **2007**, *111*, 5026−5033.